WORLD CONFERENCE ON TIMBER ENGINEERING 2025
BRISBANE, AUSTRALIA

Advancing Timber for the Future Built Environment

FORM-FITTING MASS TIMBER CONNECTIONS: WOODWORKING FOR THE NEW AGE

Maxime Daviau[1], Daniel Lacroix[2]

ABSTRACT: Current mass-timber projects rely on proprietary and carbon-intensive connectors (e.g., self-tapping screws, concealed hangers, column-to-column pillars) to resolve structural loads. Advanced manufacturing technologies enable the production of precise, complex geometries, offering the potential integration of form-fitting connections into the mass timber industry. This study investigates the behaviour, failure modes, and load-displacement characteristics of three connection geometries: a traditional mortise and tenon, multiple tenons, and a novel triangular multiple tenon design. While current code calculations predicted failure modes, they underestimated the connection capacities observed in testing. The triangular dovetail tenons demonstrated high cracking resistance, effective load redistribution post-cracking, and high post-peak strength. The study highlights the geometric sensitivity of mortise and tenon connections and the potential of the novel triangular tenon design for improved performance.

KEYWORDS: Joinery, Tenon Mortise, Timber-to-Timber, Multiple Tenons

1 – INTRODUCTION

1.1 HISTORICAL BACKGROUND

For thousands of years, wood was one of the only materials available, resulting in rich joinery cultures across the globe. The joints were commonplace in construction until the middle of the 20th century; the geometry of these connections was driven primarily by necessity and prior experience with the material [1]. The result of these joints is found in structures still standing today, such as the five-storey pagoda at Horyu-Ji in Japan, which has stood for over 1400 years, withstanding 40 large earthquakes and fire, relying solely on form-fitting timber connections [2].

Despite the substantial historical precedence, the mass timber industry relies on prefabricated proprietary connectors (e.g., self-tapping screws, beam hangers) and numerous dowel-type fasteners (e.g., bolts, screws, nails) to resolve loads. These connections, while convenient, are costly and energy-intensive, requiring a significant quantity of screws or steel to allow for load transfer. Despite this, the research and development of proprietary fasteners and connectors along with dowel-type connectors allowed designers to resolve loads without considering complex geometry, thereby accelerating the decline of traditional connections. The success and popularity of dowel-type fasteners ultimately led to codes that did not mention or provide any guidance on joinery connections, including the Canadian Standards Association (CSA) *Engineering in wood design* standard, (CSA O86) [3]. Advantages of form-fitting connections include minimal retooling costs for existing engineered wood products (EWP) manufacturers, quicker assembly, lower joint embodied energy, and the absence of numerous self-tapping fasteners, with an increasing number of projects beginning to implement these connections [e.g., 4–6].

1.2 PREVIOUS RESEARCH

The advancements of timber knowledge in terms of both research and industry have resulted in the leveraging of advanced manufacturing techniques, resulting in the development and widespread adoption of computerized-numerical-controlled (CNC) based technologies for the processing of wood. The most popular are CNC routers and milling machines, that precisely cut out wooden geometries, the most common application being those required for concealed plate and hanger-type connections. The efficiency of modern manufacturing capabilities has brought a renewed interest in form-fitting timber connections using mass timber capitalizing on these advances. Research into the impact of geometry [7,8], and the studies on embedment theory of form-fitting

[1] Maxime Daviau, Department of Civil and Environmental Engineering, University of Waterloo, Waterloo, Canada, madaviau@uwaterloo.ca

[2] Daniel Lacroix, Department of Civil and Environmental Engineering, University of Waterloo, Waterloo, Canada, daniel.lacroix@uwaterloo.ca

https://doi.org/10.52202/080513-0355

connections [9–11] are considering the anisotropic properties of wood, confirming the ability of timber joints to effectively transfer loads.

The CSA O86 code has no explicit provisions outlining a method to calculate the capacity of mortise and tenons [3]. Furthermore, the depth of any notches into the member is limited to 25% of the total member depth, restricting the ability to generate tenon geometries. Although notching depth and joinery connections are governed by the same failure principles and material strengths, the mechanisms through which multiple tenon connections fail are currently not accurately described by the code clauses and equations. Experimental investigations into the behaviour of multiple tenon connections [7], rounded dovetail connections (RDC) [8], rotational stiffness of through-tenons [10], connection stiffness in jointed panels [11], RDC flange angle [12], and varied-angle mortise and tenon connections [13] constitute the state-of-the-art in terms of modern joinery; however, they are limited in the number of specimens tested. As such, minimal experimental data on the behaviour of form-fitting timber connections, the impact of CNC milling processes on these connections, and how they compare to standard and traditional hand tools exists [1,14,15].

Digital fabrication with wood has been investigated for dimensional lumber, EWP, and heavy timbers [11,14,16,17], illustrating the versatility of modern manufacturing methodologies. Although the speed and accuracy at which joints can be made are greatly improved, a limitation of using CNC milling for connection manufacturing is the tool size and tool clearances required to fabricate the joints. Joints fabricated with advanced manufacturing techniques (e.g., CNC milling) rarely have sharp corners in both members as this requires specialized tools and post-processing [16,17]. Therefore, it is of interest to investigate form-fitting rounded geometries that can be processed quickly with minimal post-processing.

1.3 Objectives

The objective of the current test series is to investigate the impact of geometry on the capacity and deformation characteristics of form-fitting connections, leveraging digital image correlation (DIC) to understand the strain concentration and propagation over the entire beam area and not only at discrete points. Furthermore, the current test series seeks to assess if the novel tenon geometry can improve the capacity and overall deflection response as well as failure modes of form-fitting connections.

2 – FORM-FITTING CONNECTIONS

Form-fitting connections are geometries capable of providing the necessary friction forces to transfer loads between elements [18]. In the new digital age of timber construction, the elements connected through these geometries can be quickly fabricated to small enough tolerances to provide the necessary friction forces, that carpenters historically achieved through gradually shaping down the joints [1,2]. Throughout the literature and codes, the effect of these frictional forces is ignored, with designers focusing on producing joints with geometries advantageous to resolving the macroscopic forces imposed on the connection.

The experimental data around form-fitting connections illustrate the capability to transfer significant load while also deforming before failure [7,8]. Therefore, the integration of geometries capable of using frictional forces to improve the strength and deformation characteristics is of particular interest.

The most fundamental geometry used for joining elements together is the mortise and tenon, which has been used by various cultures in geographically disparate regions for centuries [1]. This type of joint is comprised of a tenon that is inserted into the mortise hole. The physical contact between the tenon and mortise allows for the load transfer between members. The joint is characterized by brittle failure of the mortise, caused by tension forces perpendicular to the grain of the mortised member, leading to a concentration of stress until crack initiation [7]. The crack from the bottom corner of the mortise will propagate parallel to the grain of the mortised member as seen in Figure 1.

Figure 1 Typical traditional failure of mortise at the bottom face.

Previous work on multiple-tenon geometry has shown that the number of tenons significantly improves the capacity while reducing the variability in load-carrying capacity of the connection [7]. Additionally, it was recommended that tenon depth and height follow a 1:1 ratio [7]. The typology of multiple tenons is of particular interest as the lower variance in predicted capacity allows for the connections to potentially move away from a

https://doi.org/10.52202/080513-0355

brittle failure mode towards a progressive failure, characterized by the embedment of the tenons and their geometry.

3 –PRELIMINARY CAPACITIES

3.1 TENON DESIGN

To understand and characterize the behaviour of mortise and tenon connections, the test series included joints fabricated with the rules of thumb that carpenters employ [1,14], recommendations for tenon geometry [7], and the findings on RDC flange angle [12]. The series investigates traditional tenons (TT), multiple tenons (MT) and triangular dovetail-shaped tenons (DT) geometries while keeping the shear area of the tenons constant as seen in Figure 2.

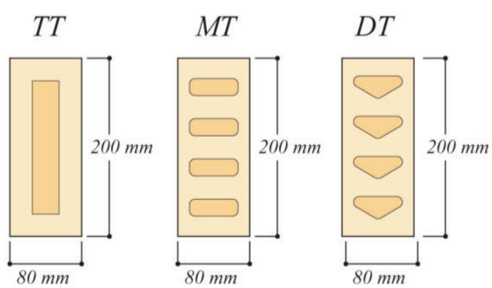

Figure 2 Tenon configuration for testing series.

3.2 TENON CAPACITY

The design of the joints for the test series was based on the availability of hand tools, the equations available in CSA O86 [3], and the national annex of Germany [19] that introduces verifications for compression strength perpendicular to grain and shear strength. The capacity of the TT, MT, and DT series was calculated by adding the capacity of each tenon based on the associated effective shear depth. This approach was used by Claus and Seim [7] and is illustrated in Figure 3 where the grey area is the portion of the section contributing to resisting the load, taken from the bottom of the tenon being considered to the top of the member.

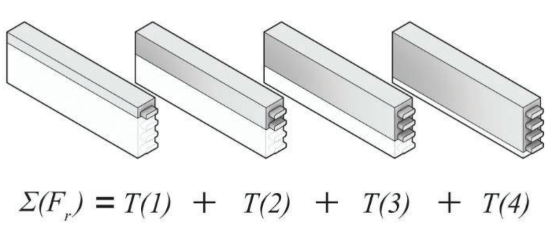

Figure 3 Multiple tenon shear depth definition d_n.

As a compression failure perpendicular to grain does not significantly impact the capacity of the connection and contributes to a ductile failure within the connection, calculation of the tenon and mortise capacity was not performed for the test series. The calculation of the tenons follows the equations for fracture shear resistance at notches (F_r) shown in (1).

$$F_r = \phi F_f A_g K_n \tag{1}$$

The equation is a function of the notch factor (K_n) defined in (2). The notch factor is based on the geometric properties of the shear depth ratio (α) as defined in (3) as a function of the member depth (d) and the notch depth (d_n), and a ratio of the notch length (e) to the member depth, shown in (4). The equation assumes that the notch length (e) is based on the distance from the inner edge of the support to the furthest edge of the notch. As this does not apply to mortise and tenon geometry, the intent behind using the clause was to apply it for a distance equal to half the tenon length.

$$K_n = 0.006d\left(1.6\left(\frac{1}{\alpha} - 1\right) + \eta^2\left(\frac{1}{\alpha^3} - 1\right)\right)^{-\frac{1}{2}} \tag{2}$$

$$\alpha = 1 - \frac{d_n}{d} \tag{3}$$

$$\eta = \frac{e}{d} \tag{4}$$

The controlling parameters are the notch length and the shear depth above the location of the underside of the tenon. The calculations indicate that the capacity of the tenons increases from the top tenon, to the bottom tenon with the implication that the top tenon is the weakest of the connection. Not captured by the design equations in CSA O86 [3] is the impact of the geometric properties of the triangular dovetail tenons. As such 1/3 from the top of the tenon was used as this represents the centroid of the tenon shape. The tenon strengths based on fracture resistance are summarized in Table 1, with tenon 1 being the single tenon in the TT series, and the highest tenon for the MT and DT series.

Table 1 Tenon capacity by location and total.

	Test Series		
Tenon	***TT (kN)***	***MT (kN)***	***DT (kN)***
1	28.5	5.4	4.9
2	-	9.4	8.9
3	-	15.0	14.2
4	-	29.9	26.7
$\Sigma(F_r)$	4.19	59.63	54.7

https://doi.org/10.52202/080513-0355

3.3 MORTISE CAPACITY

The capacity of the mortises was calculated based on the observed behaviour that the bottom of the mortise is loaded such that it is resisting tension perpendicular to the grain. As the load applied to the connection exceeds the splitting resistance of the member, crack initiation occurs and leads to tension failure along the grain as the fibres split. The splitting resistance equation in CSA O86 relates the thickness (t), member depth (d), and unloaded edge distance (e_p) as shown in (5) where the effective depth of the member (d_e) is determined by subtracting the unloaded edge distance from the total member depth.

$$QS_i = 14t\sqrt{\frac{d_e}{1-\frac{d_e}{d}}} \tag{5}$$

For multiple tenon connections, the capacity of the mortise was calculated from the bottom of the member to the bottom edge of the mortise as shown in Figure 4. For the DT series, the location of the mortise centroid was used to not be overly punitive to the mortise capacity.

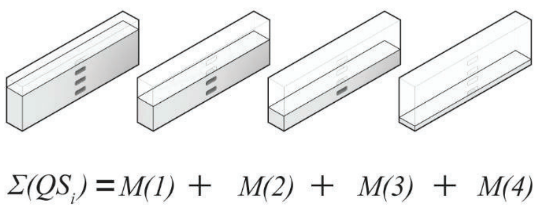

Figure 4 Multiple mortise effective member depth calculation.

The design equation for determining the splitting resistance capacity of members does account for geometric factors, such as the triangular mortises of the DT series. The angle introduced in the joint redistributes the stress from perpendicular to the grain to an angle along the length of the member. This redistribution engages a more significant portion of the cross-section, fundamentally altering the behaviour of the mortises. The results of the preliminary mortise splitting resistances are outlined in Table 2

Table 2 Mortise splitting resistance capacity by location and total.

Mortise	Test Series		
	TT (kN)	***MT (kN)***	***DT (kN)***
1	4.19	21.5	27.5
2	-	12.6	14.6
3	-	8.0	9.2
4	-	4.0	5.3
$\Sigma(QS_{ri})$	4.19	46.10	56.63

4 – TEST SET-UP

4.1 TEST SPECIMENS

The test series consisted of 9 specimens with three specimens for each of the different geometries. The specimens' cross-sections were 80 mm x 200 mm and were 600 mm in length, representing a 1:3 ratio between the height and depth of the beams. All specimens were fabricated with a combination of hand tools and power tools. This included pull saws, mitre saws, chisels, a plunge router and a table saw. The specimens were kept in an environmental conditioning chamber for 72 hours before fabrication and were fabricated in 12-hour segments once removed from the chamber to ensure that the specimens did not lose a significant amount of moisture.

The test fit process involved sanding the tenons down until the members could be inserted into the mortise with clamps or impacts from a mallet. A removable template ensured that the tenons were not undersized. The template and tenon fit are shown in Figure 5. Due to using a plunge router, the corners of the mortise were left rounded and the tenons were rounded over to match the radius of the mortise. Though the process is laborious, it is readily adapted to CNC milling or routing to a greater precision.

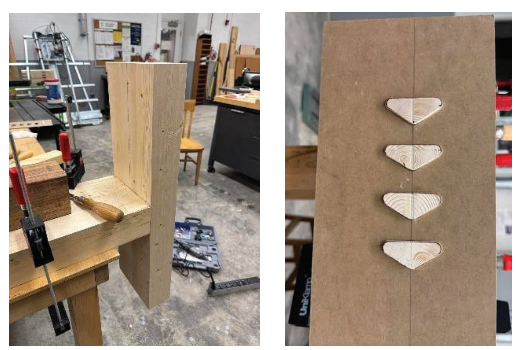

Figure 5 Test fit process during fabrication, tenon template showing DT series.

4.2 EXPERIMENTAL SET-UP

The test set-up takes precedence from ASTM D 7147 – 21, for the testing of joist hangers [20]. This informed the configuration of the beam-girder placement and the aspect ratio of the beams. The test was modified for form-fitting connections by introducing a 25 mm gap beneath the girder members to allow for the mortise to fail. Additionally, the blocking preventing torsional rotation was removed to allow for the progressive failure of the

https://doi.org/10.52202/080513-0355

beam and connection to be observed. The girders were fixed for horizontal displacement but allowed torsional rotation. The load was applied at midspan using a hydraulic Enerpac with a pin, loading a rigid steel plate to prevent local crushing of the beam member. The test set-up is shown in Figure 6. An electric pump with manual control was used to load the specimens at a relatively constant interval so that the load from the attached load cell maintained a linear slope in the elastic region. A speckle pattern was applied over the entire area of the test beam to allow for the collection of strain readings using the DIC.

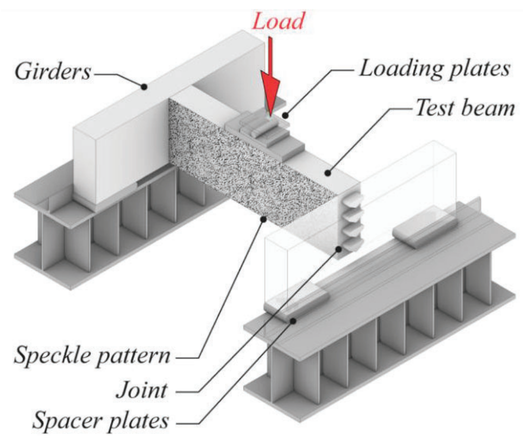

Figure 6 Test set-up for form-fitting connections.

5 – RESULTS

5.1 FAILURE MODES

The failure modes of each test series are indicative of the load redistribution within the beam as it failed. Using the DIC, the strain over the entire beam can be captured, allowing for an overall assessment of its behaviour. The strain distribution and movement during loading indicates regions where the beam is seeing higher stress and utilization and is a good predictor of failure. It was noted that the failure mode of the TT series significantly differed from the MT and DT failures as the TT series capacity was governed by failure of the mortise in the girder member, whereas the MT and DT series were governed by failure of the tenons and the beam member. The tenon did not fail in the TT series but showed crushing of the tenon.

The strain distribution throughout the cross-section right as the first cracks occur better illustrates the complex failure mechanisms observed for each test series. Figure 7, illustrates TT-02 and the respective strains right as the first crack initiates in the girder mortise. The strain distribution suggests arching or deep-beam action that directs the load toward the bottom of the tenon. This is apparent in the higher concentration of strain in these regions, connected by a strut of elevated strain from the loading point at midspan.

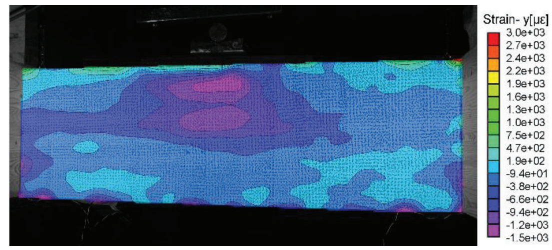

Figure 7 TT-02 at first crack initiation and propagation.

Figure 8 shows the strain distribution of MT-01 when the first crack initiates at the bottom of the top mortise. The distribution of strain is significantly more localized with a more uniform strain distribution over the cross-sectional area. As the first crack has initiated, loading of the bottom tenon has begun, resulting in the strain distribution beginning to localize in the lower region of the beam by the lowest tenon. In the TT and MT series, once the top tenon failed, the strain distribution in the lowest tenon rapidly increased, indicating that the lowest tenon was attracting more load. This eventually led to the splitting of the bottom mortise.

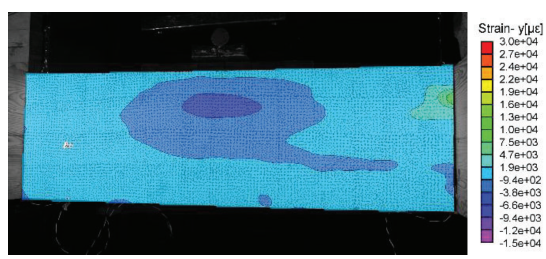

Figure 8 MT-01 prior to first crack initiation and propagation.

Figure 9 shows the strain distribution of DT-03 as the first crack initiates at the bottom of the second to the top tenon. DT-03 was the highest capacity test, and the crack initiation in in the second tenon from the top did not adversely affect the observed failure mode, and still allowed for the topmost tenon to split, with progressive failure of the remaining section afterwards. The strain distribution at the first crack shows similarities to those in Figure 8, but with higher strains in the section overall due to the higher load when the first crack occurred. Additionally, the strain pattern of the DT series when the first crack initiates is opposite to that of the TT series, indicating behaviour whereby the arching effect is avoided.

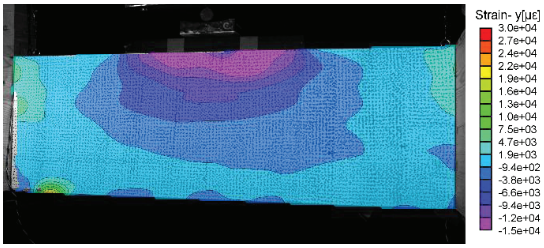

Figure 9 DT-03 at first crack initiation.

The damage to the mortises of the MT and DT series indicated different failure modes. The MT series displayed a combined failure mode, that included a typical mortise splitting failure shown in Figure 10. The mortises above the bottom mortise showed compression failures, with the second highest mortise showing a splitting failure in the direction perpendicular to the wide face of the girder. This indicates sufficient frictional forces to pull on the bottom face of the mortise with enough tension to cause a splitting failure perpendicular to grain.

Figure 10 Typical MT series mortise after failure.

The failure of the DT series indicates a redistribution of stress as the load increases resulting in a crushing failure of the lower mortises, and a progressive splitting failure of the upper mortises shown in Figure 11. Unlike the MT series, the lowest mortise did not catastrophically fail and split indicating that the mortises more effectively distributed the load through the girder cross-section.

Figure 11 Typical DT series mortise after failure.

The tenon and beam failure of the MT and DT series also indicates a significant difference in the load distribution between the members. This is most clearly observed by the different locations of splitting deformation as shown in Figure 12. The MT series showed loading of the top mortise, causing crack propagation from the underside of the mortise. Subsequent redistribution of load progressed to the lower mortises but did not allow the crack to propagate as the mortises failed allowing for shearing of the tenons between the beam and the girder.

Figure 12 Tenon Failures of MT (left) and DT series (right).

The DT series shows a similar initial failure of the top tenon, but different behaviour once the crack has initiated. The load redistributes to the next highest tenon, causing stresses to increase, eventually leading to a crack and failure along the grain. This progressive failure process is repeated until the beam member contains four significant cracks long the member extending to almost midspan from the side that failed seen in Figure 13. The splitting cracks follow the triangular shape of the tenon at each tenon, with this failure pattern being observed for each test of the DT series.

Figure 13 Typical DT series failure of beam member.

5.2 FAILURE LOAD AND DISPLACEMENT CHARACTERISTICS

The basis through which the loads is compared are based on the maximum load for each test of the series. This corresponds to the ultimate limit state (ULS) capacity of

https://doi.org/10.52202/080513-0355

the connection and members. Figure 14 shows the peak values for each test and the mean values for each tenon geometry in the testing series.

The MT and DT connections showed a significant increase in average load compared to the TT series. The MT connections had a capacity approximately three times greater than the traditional tenon with a lower spread in values. The DT series reached an average load 10% higher than the MT series, with a lower spread in capacity between the tests.

The TT series reached an average load of 14.8 kN with a coefficient of variation of 25%. The test series MT reached an average load of 68.6 kN with a coefficient of variation of 6%. The test series DT reached an average load of 75.3 kN with a coefficient of variation of 5%.

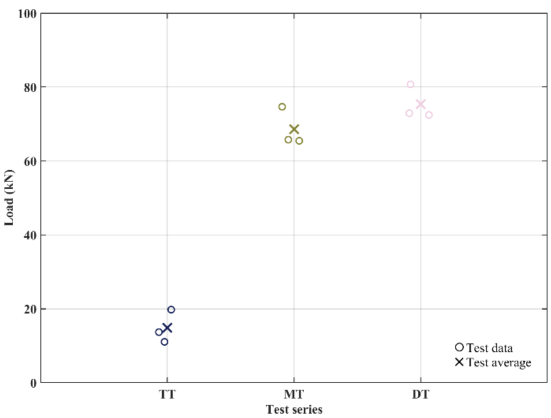

Figure 14 Peak loads and average for the three types of tenon geometries

The relative displacement between the girder and the main beam was recorded and normalized for the midspan deflection of the member. The normalized midspan deflection was chosen due to the beam's short aspect ratio and potential for failure at either end. DIC analysis was used to monitor the deflection at three locations including both ends and midspan, thereby allowing for the determination of the normalized displacement. Additionally, the complex failure mechanisms observed showed that once the load had caused the initial crack at the top member the attached string pots, connected to the top face of the member, no longer provided representative data.

Figure 15 shows the results of the TT series. The test data shows that the load increases to a peak, followed by a rapid failure. The resulting failure mode is brittle and is characterized by the splitting of the girder member at the mortise, resulting in a rapid loss of strength once the crack initiates. The splitting resistance capacity determined numerically is lower than the observed connection capacity, with the design equations correctly identifying the mortise failure as the governing failure mode.

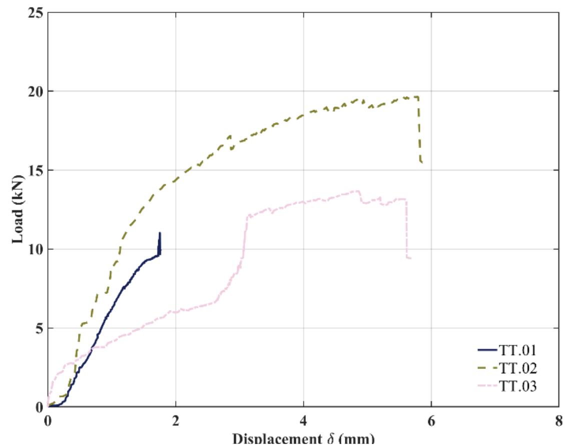

Figure 15 Load-deformation behaviour of the TT series.

The MT series displayed increased stiffness compared to the TT series reaching a higher load at a displacement of 3mm, shown in Figure 16. The first crack of the MT series develops at a significantly higher load, and results in softening of the connection. The connection begins to soften as the tenons shear, and the mortises begin to crush at the higher loads. This results in a delayed failure that is progressive in nature, allowing for post-crack strength due to the redistribution of forces within the remaining tenons.

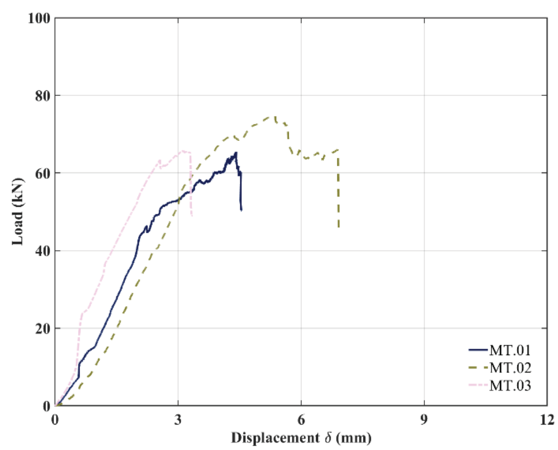

Figure 16 Load-deformation behaviour of the MT series.

As the connection displaces, the splitting resistance is exceeded, allowing for the remaining tenons to better engage. The MT series significantly softened after the top two tenons failed, resulting in a rapid progressive failure of the member. Once the top tenons split, the now stiffer bottom tenon transferred more significant force to the face of the bottom mortise, leading to the mortise failure through splitting. Furthermore, inspection of the tenons after the test indicated a shearing of the two middle tenons but not of the top and bottom tenons. Previous calculations indicated the top tenon being significantly weaker than the lower tenons, corroborating the observed failure for the top tenons, but not the middle ones.

The numerically determined capacity of the connection is lower than the experimentally observed values, with the predicted failure mode being generally correct. The behaviour of the MT series is less clearly defined by the design equations, therefore the failure of the top tenon followed by the splitting of the mortises does not significantly deviate from the expected behaviour determined numerically.

The DT series displayed similar stiffness compared to the MT series but with significantly different behaviour after the first crack initiated in the top tenon. Figure 17 shows that the first crack develops at a higher load compared to Figure 16, with the behaviour after the first crack showing significant softening and quasi-ductile behaviour as the load further increases 10 kN to 15 kN until failure. Unlike the MT series, the DT series exhibited much more post-peak deformation as the progressively failing tenons redistributed the loads to the lower tenons until the beam began to behave as four independent smaller beams. These smaller beams were impinged and held by the compressive and frictional forces of the triangular mortises. The splitting failure of the DT connection indicated that the triangular geometry of the tenon tended to dictate the splitting plane thereby resulting in an increase in the required force to generate sufficient stress to cause splitting. Furthermore, once splitting of the member occurred, the crack was able to propagate toward the midspan. The increased crack length along the beam resulted in a continuously reduced shear depth as the split sections of the beam began to behave as smaller individual beams. Due to the crushing pattern of the mortises and crushing of the tenon by the joint line, it is hypothesized that the split members began to behave as tension members, held by the triangular mortise geometry and deformed tenon.

The numerically determined capacity is lower than the testing results but captures the more balanced failure mode observed with a less clearly defined weaker member. As predicted, the top tenon splits first, followed by the successive failures of the lower tenons. Indirectly, the design equations appear to capture the behaviour of the member progressively reducing in shear depth as the split beneath the tenons extends to midspan. In contrast, the design equations did not accurately reflect the failure mode of the mortises because the interaction during failure was much more complicated than just the splitting resistance of the member.

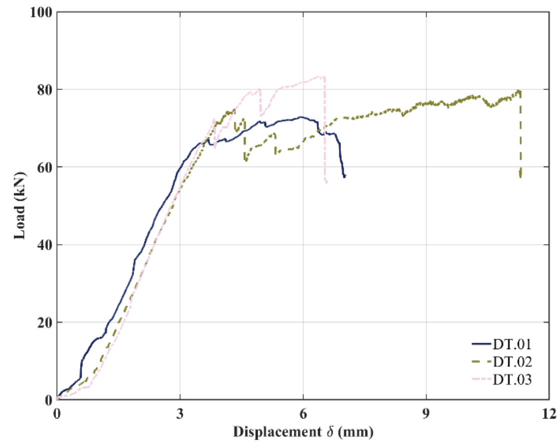

Figure 17 Load-deformation behaviour of the DT series.

6 – CONCLUSIONS

The experimental investigations on form-fitting connections show that multiple-tenon geometry has desirable characteristics regarding the load-displacement behaviour until failure. The results also corroborate the data generated by Claus and Seim [7], showing similar connection behaviour. The investigation shows that preliminary design approaches outlined in CSA O86 and Eurocode 5 [3,19] were able to inform the design and preliminary predictions of the expected failure modes of the three test series, but under-predicted their capacities.

The load-deformation behaviour of multiple tenon connections indicates that the typical brittle behaviour of traditional mortise and tenon connections can be modified to better distribute the stresses with both the tenon and mortise members, allowing for considerable deformation after the first crack occurs.

The rounded edges due to fabrication processes play a role in the stress distribution in both the tenons and mortises significantly impacting the crack location and propagation in the MT and DT series. The radius and slope of the tenon geometry should be assessed to better understand the impact of the sloped triangular geometry on the multiple tenon capacity.

The complex behaviour of multiple tenon connections

https://doi.org/10.52202/080513-0355

indicates a sensitivity to the geometric components of the mortise and tenon and should be further studied. The geometric impact should be investigated in the context of both single mortise and tenon connections to isolate the governing parameters, and the overall behaviour in multiple tenon systems to better understand the post-peak capacity of these connections and the associated deformation.

The constructability of these connections and assembly on sites is critical to the success of form-fitting connections, thus consultation with manufacturers and erectors is key in ensuring a feasible implementation of this connection typology.

7 – REFERENCES

[1] Zwerger K, Olgiati V, S̀öffker GH, Thrift P, Reisenberger J. Wood and wood joints: building traditions in Europe, Japan and China. Fourth, revised and expanded edition. Basel: Birkhäuser; 2023.

[2] 西岡常一, 1908-1995, author, 小原二郎. The building of Horyu-ji: the technique and wood that made it possible. Tokyo: Japan Publishing Industry Foundation for Culture; 2016.

[3] CSA. Engineering Design in Wood. CSA Group 2021.

[4] Shigeru Ban. Tamedia Office Building n.d.

[5] BIG. Kansas School of Architecture & Design n.d.

[6] DGJ Architektur. Collegium Academicum Student Residence n.d.

[7] Claus T, Seim W. Development of the multiple tenon timber connection based on experimental studies and FE simulation. Eng Struct 2018;173:331–9. https://doi.org/10.1016/j.engstruct.2018.06.102.

[8] Tannert T, Lam F, Vallée T. Structural performance of rounded dovetail connections: experimental and numerical investigations. Eur J Wood Wood Prod 2011;69:471–82. https://doi.org/10.1007/s00107-010-0459-1.

[9] Nguyen AC, Rezaei Rad A, Weinand Y, editors. Semi-Rigidity of Through-Tenon Joints under Tension and Shear Loads and Perpendicular-to-Grain Compression. Lausanne: Laboratory for Timber Constructions IBOIS; 2019. https://doi.org/10.5075/epfl-IBOIS-265676.

[10] Moradei DLF CT Mueller, J Brütting, C Fivet, J. Rotational stiffness in timber joinery connections: Analytical and experimental characterizations of the Nuki joint. Struct. Archit. - Bridg. Gap Crossing Bord., CRC Press; 2019.

[11] Roche S, Robeller C, Humbert L, Weinand Y. On the semi-rigidity of dovetail joint for the joinery of LVL panels. Eur J Wood Wood Prod 2015;73:667–75. https://doi.org/10.1007/s00107-015-0932-y.

[12] Tannert T, Lam F. Self-tapping screws as reinforcement for rounded dovetail connections. Struct Control Health Monit 2009;16:374–84. https://doi.org/10.1002/stc.283.

[13] Judd JP, Fonseca FS, Walker CR, Thorley PR. Tensile Strength of Varied-Angle Mortise and Tenon Connections in Timber Frames. J Struct Eng 2012;138:636–44. https://doi.org/10.1061/(ASCE)ST.1943-541X.0000468.

[14] Lukas Allner, Christoph Kaltenbrunner, Daniela Kröhnert, Philipp Reinsberg. Conceptual Joining. Basel: Birkhäuser; 2021.

[15] Hudert M, Pfeiffer S, editors. Rethinking wood: future dimensions of timber assembly. Basel, Switzerland ; Boston [Massachusetts]: Birkhauser Verlag; 2019.

[16] Gamerro J, Bocquet JF, Weinand Y. Experimental investigations on the load-carrying capacity of digitally produced wood-wood connections. Eng Struct 2020;213:110576. https://doi.org/10.1016/j.engstruct.2020.110576.

[17] Vestartas P. Design-to-Fabrication Workflow for Raw-Sawn-Timber using Joinery Solver. n.d.

[18] Van Nimwegen SE, Latteur P. A state-of-the-art review of carpentry connections: From traditional designs to emerging trends in wood-wood structural joints. J Build Eng 2023;78:107089. https://doi.org/10.1016/j.jobe.2023.107089.

[19] Eurocode 5: National Annex- Nationally determined parameters: Design of timber structures- Part1-1: General- Common rules and rules for buildings 2013.

[20] American Society for Testing and Materials (ASTM). Standard Specification for Testing and Establishing of Allowable Loads of Joist Hangars (ASTM D7147) 2021.